Journal of Solid State Chemistry 187 (2012) 177–185

Contents lists available at SciVerse ScienceDirect

Journal of Solid State Chemistry

journal homepage: www.elsevier.com/locate/jssc

Cation ordering and physicochemical characterization of the quaternary diamond-like semiconductor Ag_2CdGeS_4

Carl D. Brunetta [a], William C. Minsterman III[a], Charles H. Lake [b], Jennifer A. Aitken [a,*]

[a] Department of Chemistry and Biochemistry, Duquesne University, 600 Forbes Avenue, Pittsburgh, PA 15282, USA
[b] Department of Chemistry, Indiana University of Pennsylvania, 975 Oakland Avenue, Indiana, PA 15705, USA

ARTICLE INFO

Article history:
Received 11 October 2011
Received in revised form
22 December 2011
Accepted 23 December 2011
Available online 8 January 2012

Keywords:
Diamond-like
Semiconductor
Synchrotron powder diffraction
Wurtz-stannite
Thiogermanate
Normal tetrahedral structure

ABSTRACT

The quaternary diamond-like semiconductor, Ag_2CdGeS_4, was synthesized via high-temperature solid-state synthesis as well as structurally and physicochemically characterized. Single crystal X-ray diffraction provided a model for Ag_2CdGeS_4 in the orthorhombic, noncentrosymmetric space group $Pna2_1$ with $a=13.7415(8)$ Å, $b=8.0367(5)$ Å and $c=6.5907(4)$ Å, in contrast to a previously published model in $Pmn2_1$ from the Rietveld analysis of laboratory X-ray powder diffraction data. The $Pna2_1$ space group is supported by the Rietveld analysis of synchrotron X-ray powder diffraction data. Differential thermal analysis suggests that Ag_2CdGeS_4 exists in two polymorphs. Optical diffuse reflectance UV/vis/NIR spectroscopy indicates that the orange compound is a semiconductor with a band gap of 2.32 eV. Optical microscopy, scanning electron microscopy, energy dispersive spectroscopy and inductively coupled plasma optical emission spectroscopy were used to further characterize the material.

1. Introduction

Although quaternary diamond-like semiconductors (DLSs) were first discovered in the 1960s [1,2], these compounds have recently seen an increase in attention [3–13]. This is due to their promising, tunable properties stemming from their flexible compositions and stable structures. These normal valence compounds have structures that resemble that of either cubic or hexagonal diamond [1,2,14]. DLS compounds adhere to a series of simple guidelines, which helps to predict new compounds that will possess these structures. The first guideline is that the average number of valence electrons per ion must be 4. Next, the average valence electron concentration per anion must be 8 [1,2]. Additionally, all ions are required to be in tetrahedral environments; Pauling's rule of radius ratios (1st rule) serves as a good predictor [1,2,15]. Lastly, the octet of each anion must be fulfilled by the cations in its immediate coordination sphere, as dictated by Pauling's electrostatic valence sum rule (2nd rule) [1,2,15].

Over the years a large number of binary and ternary DLSs have been synthesized and characterized due to their relative ease of synthesis [1,2,16,17]. Although quaternary systems often present synthetic challenges, recent literature shows an amplified interested in quaternary DLSs, due to their increased compositional flexibility and technologically useful properties [6–13,17]. Provided that the guidelines of DLSs are not violated, a large number of ions can be used to construct these materials making them ideal as tunable semiconductors [7,13,18,19]. Physical properties of DLSs such as band gap [6,7,20,21], magnetism [18,22], second harmonic generation (SHG) [4,21,23] and electrical properties [16] can be tailored to a specific application by altering the composition of the material. This makes quaternary DLSs attractive materials in the areas of photovoltaics [6,7,24], spintronics [22,25], non-linear optics [4,11] and thermoelectrics [12,13,26]. However, the resulting physicochemical properties of these quaternary DLSs are not only a result of their composition, but also the structural arrangement of the ions. A universal understanding of how structure (i.e. cation ordering) is related to each of these properties is not yet known. This knowledge is necessary for materials scientists to predict applications for new DLSs. For this purpose, a complete understanding of each compound's structure as well as its physicochemical characteristics is required.

Earlier work on Ag_2CdGeS_4 by Parthè et al. [27] and Parasyuk et al. [28–30] focused only on the structure of this compound from laboratory X-ray powder diffraction data; no other properties were explored. Both of these prior studies concluded that this compound crystallizes in the orthorhombic, noncentrosymmetric space group $Pmn2_1$, a well known space group for DLSs, often called the wurtz-stannite structure [1,2,31]. A detailed comparison of the structure in $Pna2_1$ presented here, $Pmn2_1$ proposed previously [27,30], and the computationally predicted Pn space group [32] is described. Additionally this work reports diffuse reflectance UV/vis/NIR spectroscopy, differential thermal analysis, optical microscopy, scanning electron microscopy, energy dispersive

* Corresponding author. Fax: +1 412 396 5683.
E-mail address: aitkenj@duq.edu (J.A. Aitken).

0022-4596/$ - see front matter © 2012 Elsevier Inc. All rights reserved.
doi:10.1016/j.jssc.2011.12.032

spectroscopy and inductively coupled plasma optical emission spectroscopy for Ag_2CdGeS_4.

2. Experimental

2.1. Reagents

Chemicals used in this work were utilized as obtained unless otherwise noted : (1) silver powder, ~325 mesh, 99.99%, Cerac Milwaukee, WI; (2) cadmium powder, 99.999%, Strem Newburyport, MA; (3) germanium pieces were first ground using an impact mortar and pestle until the large pieces were broken up into a course powder and then ground for 5 min in a ceramic mortar and pestle before use, 99.999%, Strem Newburyport, MA; (4) sulfur powder, sublimed, 99.5%, Fisher Scientific Pittsburgh, PA.

2.2. Synthetic procedure, Ag_2CdGeS_4

Single crystals of Ag_2CdGeS_4 were produced by weighing 2 mmol of Ag, 1 mmol of Cd, 1 mmol of Ge and 4.1 mmol of S in an argon-filled glove box. These reagents were combined and ground for 20 min using an agate mortar and pestle and transferred to 9 mm o.d. fused-silica tube. The tube was then flame-sealed under a vacuum of approximately 10^{-3} mbar and placed in a programmable furnace. The sample was heated to 800 °C over 12 h and held at that temperature for 96 h. After a slow cooling step of 5 °C/h (60 h) to 500 °C, the sample was allowed to cool to ambient temperature. Next the tube was opened and the content was examined with a light microscope. The product was comprised of mostly orange crystals and a small amount of dark green and red crystals. X-ray powder diffraction and energy dispersive spectroscopy indicated that the orange crystals were Ag_2CdGeS_4. Using the same techniques, the red crystals were identified as Ag_8GeS_6 [33] and the dark green crystals were determined to be an unidentified cadmium–germanium–sulfide phase. Both ternary phases were manually separated from the orange crystals under a light microscope. Analysis of the ground hand-selected, orange crystals by synchrotron X-ray powder diffraction showed that the large majority of the sample consisted of Ag_2CdGeS_4 and only trace amounts (less than 1%) of germanium sulfide and germanium.

2.3. Physical property measurements

2.3.1. Optical microscopy

Optical images were collected using a Keyence Digital Microscope System, VHX-600. Images with increased depth of field were obtained using the Keyence Profile Measurement Unit VHX-S15 with an antivibration system. The Keyence VH-Z100R Real Zoom Lens with magnification range of ×100– ×1000 was used.

2.3.2. Scanning electron microscopy and energy dispersive spectroscopy (SEM/EDS)

SEM/EDS was performed on a Hitachi S-3400N scanning electron microscope equipped with a Bruker Quantax model 400 energy dispersive spectrometer using an XFlash® 5010 EDS detector with a 129 eV resolution. Samples were mounted on double-sided carbon tape affixed to an aluminum specimen holder. Images were taken at a working distance of 10 mm with an accelerating voltage ranging from 2.5 to 15 kV. EDS spectra were also collected at a working distance of 10 mm and an accelerating voltage of 15 kV for 3 min live time.

2.3.3. Inductively coupled plasma optical emission spectroscopy (ICP-OES)

Quantitative analysis of Ag, Cd, Ge and S was performed by RJ Lee Group Inc. (Monroeville, PA) using inductivity coupled plasma optical emission spectrometry (ICP-OES). Samples were prepared for analysis via a microwave-assisted acid digestion. High-pressure XP1500 vessels in a MarsExpress CEM Microwave system were used. The digested samples were analyzed in a Varian 730ES ICP-OES for Ag, Cd, Ge and S. The recovery was quantitative.

2.3.4. Single-crystal X-ray diffraction data collection and reduction

A Bruker SMART Apex 2 CCD single crystal X-ray diffractometer using graphite monochromatized molybdenum $K\alpha$ radiation was used to collect data at ambient temperature. Data were collected with a tube power of 50 kV and 30 mA for 35 s per frame. SAINT was used to integrate the data and SADABS was employed to perform the absorption correction [34,35]. XPREP was used for space group determination and to create files for SHELXTL. Based on systematic absences, two space groups were initially considered, $Pna2_1$ and $Pnma$. The space group $Pna2_1$ (No. 33) was selected because all DLSs are noncentrosymmetric. The additional systematic absences, $h0l$ for $h=2n+1$, clearly supported $Pna2_1$ over the previously reported $Pmn2_1$.

2.3.5. Single crystal structure solution and refinement

The SHELXTL-PC [36] software package was used to solve and refine the crystal structure, Fig. 1. All atoms were located at general positions. The sites occupied by the Ag^{1+} and Cd^{2+} ions were nearly indistinguishable due to these ions being isoelectronic, with nearly identical X-ray scattering factors and similar coordination geometries.

Various arrangements of Ag^{1+} and Cd^{2+} ions were refined at the three nearly identical 46 electron peaks in the electron density maps, maintaining a 2:1 ratio of ions (both disordered and ordered models were investigated). The best model determined from refinement of the single crystal X-ray diffraction data is denoted as model S. Crystallographic details are reported in Table 1. Table 2 lists the refined atomic coordinates and isotropic displacement parameters for

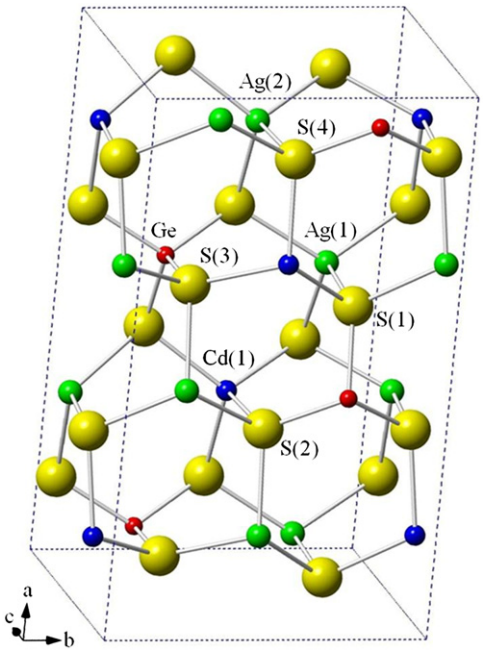

Fig. 1. $Pna2_1$ structure of Ag_2CdGeS_4 (model S) viewed slightly tilted from the crystallographic c-axis.

model S as well as alternative assignments of the cations that were considered, denoted as S′ and S″.

An alternative structure model was obtained from the structure solution (expo2009) [37] and Rietveld refinement (GSAS/EXPGUI) [38,39] of synchrotron X-ray powder diffraction data and will be referred to as model P. This model, also in $Pna2_1$, possesses an alternate set of cation sites distributed amongst a hexagonally closest-packed network of sulfide ions, Fig. 2. Model P, which will be further discussed in the results and discussion section, converged with Rp=7.46% in GSAS/EXPGUI. Refinement of model P using the single crystal X-ray diffraction data refined with $R1(I>2\sigma(I))=6.10\%$.

After the use of chemical reasoning and the Hamilton R test [40,41], model S was determined to be most probable structure.

Table 1
Crystallographic data and experimental details for Ag_2CdGeS_4 (model S).

Empirical formula	Ag_2CdGeS_4
Size	$0.21\times0.11\times0.05$ mm^3
Color	Orange
Habit	Rod
Formula weight	528.97
Temperature	296(2) K
Wavelength	0.71073 Å
Space group	$Pna2_1$
Unit cell dimensions	$a=13.7415(8)$ Å
	$b=8.0367(5)$ Å
	$c=6.5907(4)$ Å
	$\alpha=\beta=\gamma=90^\circ$
Volume	727.85(8) Å^3
Z	4
Calculated density	4.827 mg m^{-3}
Flack parameter	0.03(1)
$F(000)$	952
Reflections collected/independent	9573/1600
Data/restraints/parameters	1600/1/75
Completeness to theta=27.07	100.0%
Goodness of fit	1.112
Final R indices [$I>2$sigma(I)]	$R1=0.0235$, $wR^2=0.0583$
R indices (all data)	$R1=0.0267$, $wR^2=0.0620$
Largest peak/hole	1.43/−0.56 eÅ^{-3}

Refinement of F^2 was made against all reflections.

$$R_1=\frac{\sum||F_O|-|F_C||}{\sum|F_O|},\quad wR_2=\sqrt{\frac{\sum[w(F_O^2-F_C^2)^2]}{\sum[w(F_O^2)^2]}},\quad w=\frac{1}{(\sigma^2(F_O^2)+(aF_O)^2+bp]},$$

$$P=[2F_C^2+Max(F_O^2,0)]/3.$$

Table 2
$M(1)$, $M(2)$ and $M(3)$ assignments for several structural models and fractional atomic coordinates and equivalent isotropic displacement parameters (Å$^2\times10^3$) for Ag_2CdGeS_4 (model S).

Site	Model S	Model S′	Model S″	SOF	Model SD*	SOF
$M(1)$	Ag(1)	Cd(1)	Ag(1)	1	Ag(1)	1
$M(2)$	Ag(2)	Ag(2)	Cd(1)	1	Ag(2)	0.83
					Cd(2)	0.17
$M(3)$	Cd(1)	Ag(1)	Ag(2)	1	Ag(3)	0.17
					Cd(3)	0.83
Site	x	y	z	$U_{(eq)}$**		
$M(1)$	0.42446(4)	0.23807(5)	0.2165(1)	40(1)		
$M(2)$	0.15876(3)	0.49941(5)	0.1976(1)	38(1)		
$M(3)$	0.34215(2)	0.48665(4)	0.70491(8)	22(1)		
Ge(1)	0.09086(3)	0.24090(5)	0.7118(1)	13(1)		
S(1)	0.4403(1)	0.2426(1)	0.8286(3)	19(1)		
S(2)	0.16390(9)	0.0134(1)	0.8216(3)	19(1)		
S(3)	0.0931(1)	0.2432(1)	0.3753(3)	20(1)		
S(4)	0.16580(8)	0.4696(1)	0.8176(3)	18(1)		

* Model SD is a disordered version of model S.
** $U_{(eq)}$ is defined as 1/3 the trace of the orthogonal tensor U_{ij}.

The ratio of $wR2$(S)/$wR2$(P) was determined to be 2.166, greater than the Hamilton confidence level for 99.5% certainty of 1.034. This test was employed for all models considered, see Table 3. Only the disordered model, SD, failed the Hamilton test indicating that it could not be rejected at 99.5% certainty.

2.3.6. Synchrotron X-ray powder diffraction

High resolution synchrotron X-ray powder diffraction data were collected using beamline 11-BM at the Advanced Photon Source (APS), Argonne National Laboratory using an average wavelength of 0.413838 Å. Discrete detectors covering an angular range from −6 to 16° 2θ were scanned over a 34° 2θ range, with data points collected every 0.001° 2θ and a scan speed of 0.01°/s.

The 11-BM instrument uses X-ray optics with two platinum-striped mirrors and a double-crystal Si(111) monochromator, where the second crystal has an adjustable sagittal bend [42]. Ion chambers monitor incident flux. A vertical Huber 480 goniometer, equipped with a eidenhain encoder, positions an analyzer system comprised of twelve perfect Si(111) analyzers and twelve Oxford–Danfysik $LaCl_3$ scintillators, with a spacing of 2° 2θ [43]. The sample was spun during data collection. A Mitsubishi robotic arm was used to mount and dismount the sample on the diffractometer [42]. An Oxford Cryosystems, Cryostream Plus device, was used to maintain the sample temperature at 100 K.

The diffractometer was controlled via EPICS [44]. Data were collected while continually scanning the diffractometer 2θ arm. A mixture of NIST standard reference materials, Si (SRM 640c) and Al_2O_3 (SRM 676), was used to calibrate the instrument, where the Si lattice constant determines the wavelength for each detector. Corrections were applied for detector sensitivity, 2θ offset, small differences in wavelength between detectors, and the source intensity, as noted by the ion chamber before merging the data into a single set of intensities evenly spaced in 2θ.

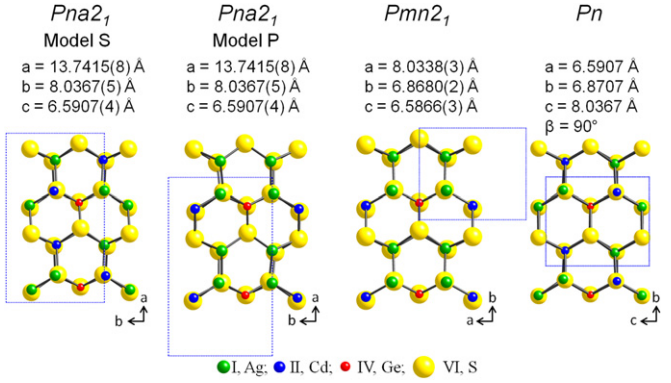

Fig. 2. Structural comparison of Ag_2CdGeS_4 in space groups $Pna2_1$, $Pmn2_1$ and Pn.

Table 3
Results of the Hamilton R test [40], which compares the weighted R factors determined from refinement of several structural models using single crystal X-ray diffraction data to that of model S.

Model	Cd	Ag	$R1$ ($I>2\sigma(I)$)	$wR2$ (all data)	$wR2$ ratio	$\mathcal{R}'$
S	$M(3)$	$M(1)$, $M(2)$	0.0235	0.0620	N/A	N/A
S′	$M(1)$	$M(2)$, $M(3)$	0.0280	0.1240	1.997	1.034
S″	$M(2)$	$M(1)$, $M(3)$	0.0266	0.1256	2.023	1.034
SD	$M(2)$, $M(3)$	$M(1)$, $M(2)$, $M(3)$	0.0236	0.0622	1.002	1.004
P*	N/A	N/A	0.0610	0.1343	2.166	1.034

* The cations reside in different crystallographic sites in model P and cannot be directly compared to sites $M(1)$, $M(2)$ and $M(3)$.

The data were indexed with N-TREOR in expo2009 [37] and the lattice parameters were refined with GSAS/EXPGUI [38,39] to $a=13.7407(1)$ Å, $b=8.0164(1)$ Å, $c=6.5927(1)$ Å, $\alpha=\beta=\gamma=90^\circ$. The structure was solved with expo2009 and Rietveld refinement was accomplished with GSAS/EXPGUI. The space group was determined as $Pna2_1$ based on systematic absences. Eight atoms were located in general positions resulting in model P. Additionally, Rietveld refinements in GSAS/EXPGUI were carried out using model S, which was determined from single crystal X-ray diffraction data.

The background was fitted with a shifted Chebyschev polynomial with ten terms [45]. For both models, Ag^{1+} and Cd^{2+} ions were refined anisiotropically; but, all other atoms were refined isotropically and independently. With this high-quality data, the profiles (i.e. peak shape) are determined more by the sample than the instrument profile and therefore better described by the Lorentzian terms. The reflection profiles contained a significant amount of anisotropic strain broadening, which was refined. All data were corrected for absorption with the absorption coefficient being refined to 10.29. All structure factors were corrected for $\Delta F'$ and $i\Delta F''$ (anomalous dispersion coefficients). Models S and P were used as starting models for Rietveld analysis. Both models converged with similar statistics. For model S the least squares refinement converged with $\chi^2=1.423$, Rp=7.45% (all data) and wRp=9.65% (all data), while that of model P converged with $\chi^2=1.426$, Rp=7.46% (all data) and wRp=9.66% (all data). These two models in $Pna2_1$ are virtually indistinguishable with powder diffraction data.

2.3.7. Diffuse reflectance UV/vis/NIR spectroscopy

Diffuse reflectance UV/vis/NIR spectra were collected using a Varian Cary 5000 spectrometer equipped with a Harrick Praying Mantis diffuse reflectance accessory. The sample was ground, placed in the sample cup and compared to a similarly prepared 100% reflectance standard, $BaSO_4$. Data were collected from 2500 to 200 nm at a scan rate of 600 nm/min. The collected percent reflectance was converted to absorption using the Kubelka–Munk equation [46] and wavelength was converted to eV.

2.3.8. Differential thermal analysis (DTA)

Thermal studies were carried out on a Shimadzu DTA-50 thermal analyzer using an Al_2O_3 reference that has no thermal events over the studied range of 25–1000 °C. The instrument was calibrated using a three-point method utilizing the melting points of indium, zinc and gold standards. Both the reference and the sample of comparable mass were vacuum-sealed in fused-silica ampoules and placed in the instrument. The ampoules were then heated at a rate of 10 °C/min to 1000 °C, held at that temperature for 1 min, and cooled at a rate of 10 °C/min to 100 °C. This cycle was repeated to distinguish between reversible and irreversible events. DTA residues were further characterized using X-ray powder diffraction.

3. Results and discussion

3.1. Morphology and composition

Optical microscopy was used to image the orange Ag_2CdGeS_4 crystals and the differently colored crystals of the unwanted phases. The colors of these materials are prominently different; examples can be found in Fig. 3a and b. These crystals were also imaged with SEM to more carefully study size and morphology. In addition to the noticeable difference in color, the ternary and quaternary phases also have dissimilar habits. The orange crystals are found as single flat needles or in large bundles of planks, while the darker colored crystals form as polyhedra with rounded corners, Fig. 3c and d. Sizable crystals of the orange phase were shown to be as long as 1 mm in length while the average size was approximately

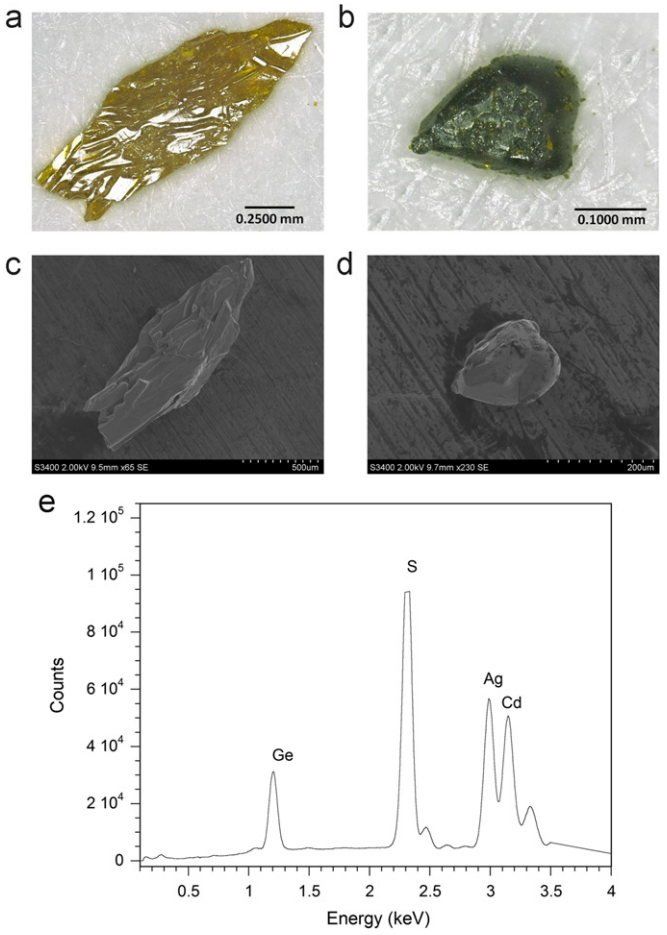

Fig. 3. (a) Digital image of an orange Ag_2CdGeS_4 crystal, (b) digital image of the darker Cd–Ge–S phase, (c) SEM micrograph of an orange crystal taken with a magnification of 65×, (d) SEM micrograph of a dark crystal taken with a magnification of 230× and (e) EDS spectra of the orange crystal with the major peak of each element labeled.

$600\times150\ \mu m^2$. Crystals of the darker colored ternary phases were found to have an average size of $450\times450\ \mu m^2$. These sizes proved to be large enough that the samples could be physically separated under a light microscope using a needle. EDS spectra showed the presence of all four elements in the orange crystals and only three of the intended elements on clean regions of the darker material, Fig. 3e. Since EDS is only semi-quantitative, the composition of the hand-selected orange crystals was confirmed using ICP-OES. The ICP-OES results yielded a stoichiometry of $Ag_{1.96}Cd_{1.04}Ge_{0.84}S_4$, in relatively close agreement with our predicted formula of Ag_2CdGeS_4.

3.2. Structure

3.2.1. Structure determination challenges

The structure determination of Ag_2CdGeS_4 is difficult due to Ag^{1+} and Cd^{2+} being isoelectronic. As a result, the calculated X-ray powder diffraction patterns for the compound in the three space groups that were considered, $Pna2_1$, $Pmn2_1$ [30] and Pc [32], are extremely similar, with additional low intensity peaks and slight intensity changes among common peaks being the only differences present in the calculated patterns. These subtle variations result from differences in the environments around the anion sites as a consequence of the different cation ordering and are manifested in the structure factors. When comparing Ag^{1+} and Cd^{2+} their atomic X-ray scattering factors are nearly identical,

with a less than 5% difference [32,47]. However the environments surrounding each of the cations in the proposed structures in question are different, which leads to subtle differences in the X-ray structure factors, the resulting symmetry and X-ray powder diffraction patterns. These subtle differences were closely examined in an effort to determine the most favorable structure.

Unfortunately, these types of indicators are extremely challenging to observe. Small diffraction peaks of ~1% or less in relative intensity are usually lost in the background of laboratory-collected powder X-ray diffraction data. Additionally, subtle differences in peak intensities can often be attributed to powder sample preparation, which can frequently result in preferred orientation. If these differences are to be used to distinguish between the different structure models, it would be with the use of high-quality powder (i.e. synchrotron) or single crystal X-ray diffraction data. This is because the difference in Ag^{1+} and Cd^{2+} atomic scattering factors for a given reflection increases with decreasing wavelength [47]. Additionally the use of lower wavelengths gives rise to higher resolution data.

3.2.2. Structure description

As determined from single crystal X-ray diffraction data, Ag_2CdGeS_4 crystallizes in the orthorhombic noncentrosymetric space group $Pna2_1$. In this structure, all ions are tetrahedrally coordinated and reside in general positions. Due to the difficulty of discerning Ag^{1+} and Cd^{2+} using X-ray data, three ordered structure models that place Cd on the $M(1)$ site (model S′), on the $M(2)$ site (model S″) and on the $M(3)$ site (model S) were considered, Table 2. Models S′ and S″ refined with higher weighted R factors and were deemed inferior to model S by use of the Hamilton R factor significance test, Table 3 [40]. In model S each sulfur anion is surrounded by two silver cations, one cadmium cation and one germanium cation in accordance to Pauling's 2nd rule of local electroneutrality [15]. Bond distances in Table 4 show an average Ag–S bond length of 2.576(2) Å for Ag(1) and 2.539(3) Å for Ag(2). These distances compare well to those found for the quaternary DLS compounds $AgCd_2GaS_4$ with an average Ag–S bond length of 2.550(2) Å [48], Ag_2HgSnS_4 with an average Ag–S bond length of 2.43(2) Å [49] and Ag_2ZnGeS_4 with an average Ag–S bond length of 2.578(5) Å [50]. The Cd–S bond has an average length of 2.526(2) Å, while the Ge–S bond lengths average 2.214(3) Å. These results are in agreement with bond lengths measured in the chemically related DLS Cu_2CdGeS_4, 2.528(6) Å and 2.28(1) Å, respectively [51].

The structure of Ag_2CdGeS_4 can be described as a hexagonal, closest-packed array of sulfur anions with Ag^{1+}, Cd^{2+} and Ge^{4+} occupying tetrahedral holes. The model S structure of Ag_2CdGeS_4 is isostructural to the DLS Li_2CoSiO_4 [52]. The structure can be viewed as a corner-sharing, three-dimensional network of MS_4 tetrahedra. The CdS_4 tetrahedra are isolated from one another, as are the GeS_4. The $Ag(1,2)S_4$ alone form a 3-dimensional network, where each AgS_4 connects to four others by sharing corners. When viewed down the a-axis one can see (Fig. 4) the alternating nature of the cations. Rows along the c-axis of alternating Ag(1)–S_4 and Ge(1)–S_4 tetrahedra (ABAB) are separated by rows of Ag(2)–S_4 and Cd(1)–S_4 tetrahedra (CDCD). The pattern is then alternated (BABA) and (DCDC) after which it repeats.

Table 4
Selected bond distances (Å) and angles (deg.) for Ag_2CdGeS_4 (model S).

Ag(1)–S(1)	2.566(1)	S(1)–Ag(1)–S(2)	106.91(5)
Ag(1)–S(2)	2.617(1)	S(1)–Ag(1)–S(3)	109.38(6)
Ag(1)–S(3)	2.546(1)	S(1)–Ag(1)–S(4)	108.06(5)
Ag(1)–S(4)	2.575(1)	S(2)–Ag(1)–S(3)	105.27(5)
		S(2)–Ag(1)–S(4)	114.60(6)
		S(3)–Ag(1)–S(4)	112.42(5)
Ag(2)–S(1)	2.532(1)	S(1)–Ag(2)–S(2)	111.52(5)
Ag(2)–S(2)	2.572(1)	S(1)–Ag(2)–S(3)	106.13(6)
Ag(2)–S(3)	2.535(1)	S(1)–Ag(2)–S(4)	115.65(6)
Ag(2)–S(4)	2.518(2)	S(2)–Ag(2)–S(3)	103.09(6)
		S(2)–Ag(2)–S(4)	106.48(5)
		S(3)–Ag(2)–S(4)	113.34(5)
Cd(1)–S(1)	2.516(1)	S(1)–Cd(1)–S(2)	113.98(5)
Cd(1)–S(2)	2.536(1)	S(1)–Cd(1)–S(3)	107.77(5)
Cd(1)–S(3)	2.511(1)	S(1)–Cd(1)–S(4)	112.00(5)
Cd(1)–S(4)	2.539(1)	S(2)–Cd(1)–S(3)	112.80(5)
		S(2)–Cd(1)–S(4)	105.35(5)
		S(3)–Cd(1)–S(4)	104.59(5)
Ge(1)–S(1)	2.212(1)	S(1)–Ge(1)–S(2)	111.18(6)
Ge(1)–S(2)	2.207(1)	S(1)–Ge(1)–S(3)	111.09(7)
Ge(1)–S(3)	2.218(2)	S(1)–Ge(1)–S(4)	105.96(6)
Ge(1)–S(4)	2.219(1)	S(2)–Ge(1)–S(3)	109.18(7)
		S(2)–Ge(1)–S(4)	111.85(6)
		S(3)–Ge(1)–S(4)	107.51(6)

3.2.3. Comparison of $Pmn2_1$, $Pna2_1$ and Pc (Pn) structures for Ag_2CdGeS_4

The space group $Pna2_1$ has been observed for quaternary oxides, for example Li_2CoSiO_4 [52]. Although relatively rare among quaternary DLSs, $Pna2_1$ is a common space group for ternary DLSs, such as $AgInS_2$ [53] and $LiGaS_2$ [54]. However this is not the only space group proposed for Ag_2CdGeS_4, Fig. 2.

In 1969, Parthé et al. reported a wurtz-stannite structure, in space group $Pmn2_1$, and lattice parameters for Ag_2CdGeS_4 from laboratory X-ray powder diffraction data [27]. Later in 2005, Parasyuk et al. supported the same space group with a refined structure from laboratory X-ray powder diffraction data [30]. The space group $Pmn2_1$ is a well-known space group for DLSs, such as Cu_2CdGeS_4 [55] and Cu_2ZnSiS_4 [5]. Additionally, a computational study in 2010 by Chen et al. predicted the Pc space group for Ag_2CdGeS_4 from Madelung energy calculations [32]. This structure has been observed for other DLSs, first reported in 1969 for Na_2ZnSiO_4 [56] and more recently for the compound Li_2ZnSnS_4 [3]. The prediction was made by comparing Madelung energies for possible structures abiding by the diamond-like rules and a $2\times2\times1$ supercell of wurtzite [32]. Although $Pna2_1$ satisfies the rules of diamond-like materials, it has a larger supercell of $4\times2\times1$ and was not considered in Chen's study. The main difference between the structures reported in $Pna2_1$, $Pmn2_1$ and Pc (Pn) is the arrangement of the cations.

The difference in the cation arrangement of the $Pmn2_1$ and $Pna2_1$ models is best illustrated by the polyhedral view of the two structures shown in Fig. 4. In this view both structures are oriented with the tetrahedra pointing in the same direction demonstrating the lack of an inversion center in both structures. It is also easy to notice the higher symmetry of the $Pna2_1$ structure from this view. When comparing the crystallographic sites of the $Pna2_1$ structure to those found in $Pmn2_1$, it can be seen that both structures possess one crystallographically unique Ge. Closer examination of the GeS_4 tetrahedra viewed down each corresponding axis shows that the arrangement of the isolated GeS_4 tetrahedra are identical. Further comparisons were made with the one crystallographically unique Cd in each structure. However, the positions of the Cd atoms relative to the GeS_4 tetrahedra are different, demonstrating that the Cd sites in the two models are not equivalent, Fig. 2.

Another model for consideration in the space group $Pna2_1$, model P, was obtained from the solution of the synchrotron powder diffraction data. In this structure looking down the a-axis there are rows along the a-axis of alternating Cd(1)–S_4 and Ge(1)–S_4 tetrahedra (ABAB) separated by rows of Ag(1)–S_4 and Ag(2)–S_4 tetrahedra (CDCD). The pattern is then alternated (BABA) and (DCDC) after which it repeats. While this structure has the same general pattern as model S, the ions that make up the pattern are

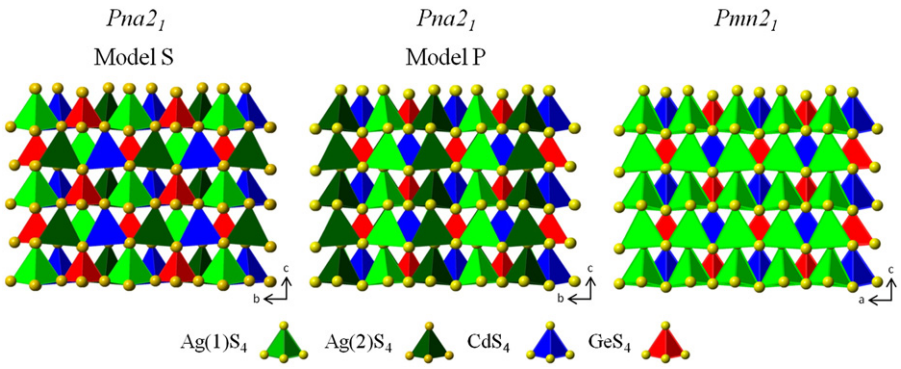

Fig. 4. Polyhedral representation of Ag_2CdGeS_4 in $Pna2_1$ (models S and P) and $Pmn2_1$ viewed down an equivalent axis.

different, Figs. 2 and 4. We were unable to find any compound in the literature possessing this structure type. The major difference between model P and model S is that in model S each crystallographicaly unique sulfur anion is surrounded by one of each of the crystallographically unique cations, Ag(1), Ag(2), Cd(1) and Ge(1). However, in model P, one unique sulfur anion is surrounded by Ag(1), Ag(1), Cd(1) and Ge(1) while another one is surrounded by Ag(2), Ag(2), Cd(1) and Ge(1). The other two sulfur anions are connected to one of each of the unique cations. Therefore, although both models contain a hexagonally closest packed array of sulfur anions, the pattern of the crystallographically unique sulfur anions is not the same in the two structure models. At first glance, model P looks very similar to the model in $Pmn2_1$. If only the cation sites are considered, it becomes obvious that the one crystallographically unique Ag in the $Pmn2_1$ structure splits into two crystallographically unique Ag cations in model P. However, that is not the only difference. If the sulfur ions are examined more closely, it can be found that the number of crystallographically unique sulfur sites is different (3 for $Pmn2_1$ and 4 for $Pna2_1$) and the sulfur anions are arranged in a different pattern in order to generate the hexagonally closest packed array.

A model of Ag_2CdGeS_4 was constructed in the *Pn* space group, an equivalent space group (different setting) to the predicted *Pc* [32,57]. Comparison of this model to the $Pna2_1$ structure shows that the locations of the Cd cations in relation to the GeS_4 tetrahedra are not equivalent, which is also found in the comparison to the $Pmn2_1$ model. The AgS_4 tetrahedra in the *Pn* model are aligned in diagonal columns in the *ac* plane in contrast to the herringbone configuration in the $Pna2_1$ model found in the equivalent *bc* plane.

Another major difference between the models of $Pna2_1$, $Pmn2_1$ and *Pn* is the larger unit cell found for the $Pna2_1$ model. This may introduce the concern that the measured doubled axis from the single crystal X-ray diffraction data may be not be "real". To check this, careful analysis of the reflections from the single crystal X-ray diffraction data and their *hkl* indexes was performed. Since the *h* parameter corresponds to the doubled axis, the data were separated into odd and even *h* values. Then the measured intensity was compared to the background to determine how many reflections were greater than 4σ. If the data collected only showed measurable intensity from the even sets of *h* values, it could be evidence that the doubled axis is not real. However, this analysis showed the presence of reflections greater than 4σ for both groups, even and odd. Out of 6954 reflections with intensities greater than 4σ, 51.6% had odd *h* values.

3.3. X-ray powder diffraction

The synchrotron X-ray powder diffraction data set clearly showed the low intensity peaks not present in the laboratory-collected X-ray powder diffraction data. Additionally, the systematic absences for the *n*-glide perpendicular to the *a*-axis (0*kl* for $k+l=2n+1$), the *a*-glide perpendicular to the *b*-axis (*h*0*l* for $h=2n+1$) and the 2_1 screw axis along the *c*-axis (00*k* for $k=2n+1$) are clearly apparent in this data set. Interestingly, the structure that was initially solved from the synchrotron X-ray powder diffraction data, model P, is not the same as the preferred model as determined from single crystal X-ray diffraction, model S. When refined against the synchrotron X-ray powder diffraction data, model S and model P are indistinguishable and gave virtually identical statistics and features on the difference Fourier map. This may be indicative of both phases being present in the powder. On the other hand, when model P was refined against the single crystal X-ray data, the statistics are reasonable and the model makes chemical sense; however, the statistics for model S are clearly favored as discussed previously. The Rietveld plot of the synchrotron X-ray powder diffraction data using model S as a starting model is shown in Fig. 5. While the proposition of yet another structural model adds additional ambiguity to the structure determination of Ag_2CdGeS_4, two things are clearly evident from this data: (1) the larger unit cell is confirmed and (2) the presence of the higher symmetry is apparent.

3.4. Differential thermal analysis (DTA)

DTA of a ground sample of Ag_2CdGeS_4, Fig. 6, shows a broad endothermic event that we believe to be a phase transition to another polymorph followed by a melting point. Upon cooling, the high-temperature phase recrystallizes and then transitions back to the original structure. In the second cycle of the DTA, the phase transition and melting points are more clearly defined. X-ray powder diffraction of the DTA residue, Fig. 7, shows that we obtain the same diffraction pattern for the Ag_2CdGeS_4 sample after the experiment, supporting the phase transition hypothesis presented above. This is very interesting because this leaves the possibility open that Ag_2CdGeS_4 might exist in another structure. In both the publications by Parthé et al. [27] and Parasyuk et al. [30] the authors were not specific about the synthetic conditions used to prepare Ag_2CdGeS_4, so it is not possible to directly compare our synthetic procedures. In this study a second phase of Ag_2CdGeS_4 was never observed. Reactions carried out at higher temperatures always produced additional quantities of the unwanted Ag_8GeS_6 phase. Reactions quenched from high temperature yielded almost no Ag_2CdGeS_4, but rather a mixture of Ag_8GeS_6, Ag_2S, GeS_2, Ag_5Cd_8 and a few unidentified diffraction peaks. Interestingly, high-temperature polymorphs are usually of higher symmetry than lower temperature phases. In this work crystals have been isolated with the highest symmetry structure that has been reported for Ag_2CdGeS_4.

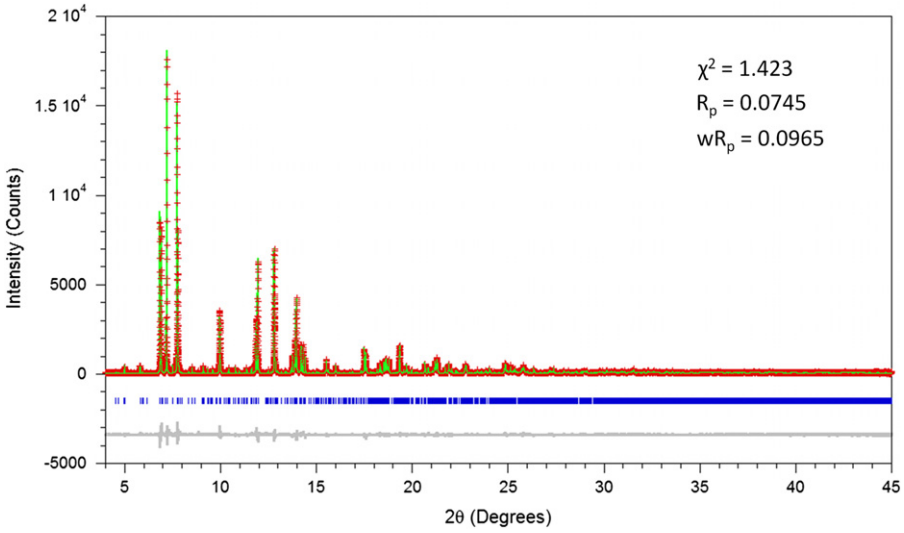

Fig. 5. Rietveld refinement of Ag_2CdGeS_4 refined in *Pna*2_1 (model S) using synchrotron X-ray powder diffraction data. The observed data (+++) and calculated data (solid line) are overlaid at the top. While tick marks (|||) indicating calculated peak locations and a difference plot (solid line) are shown below.

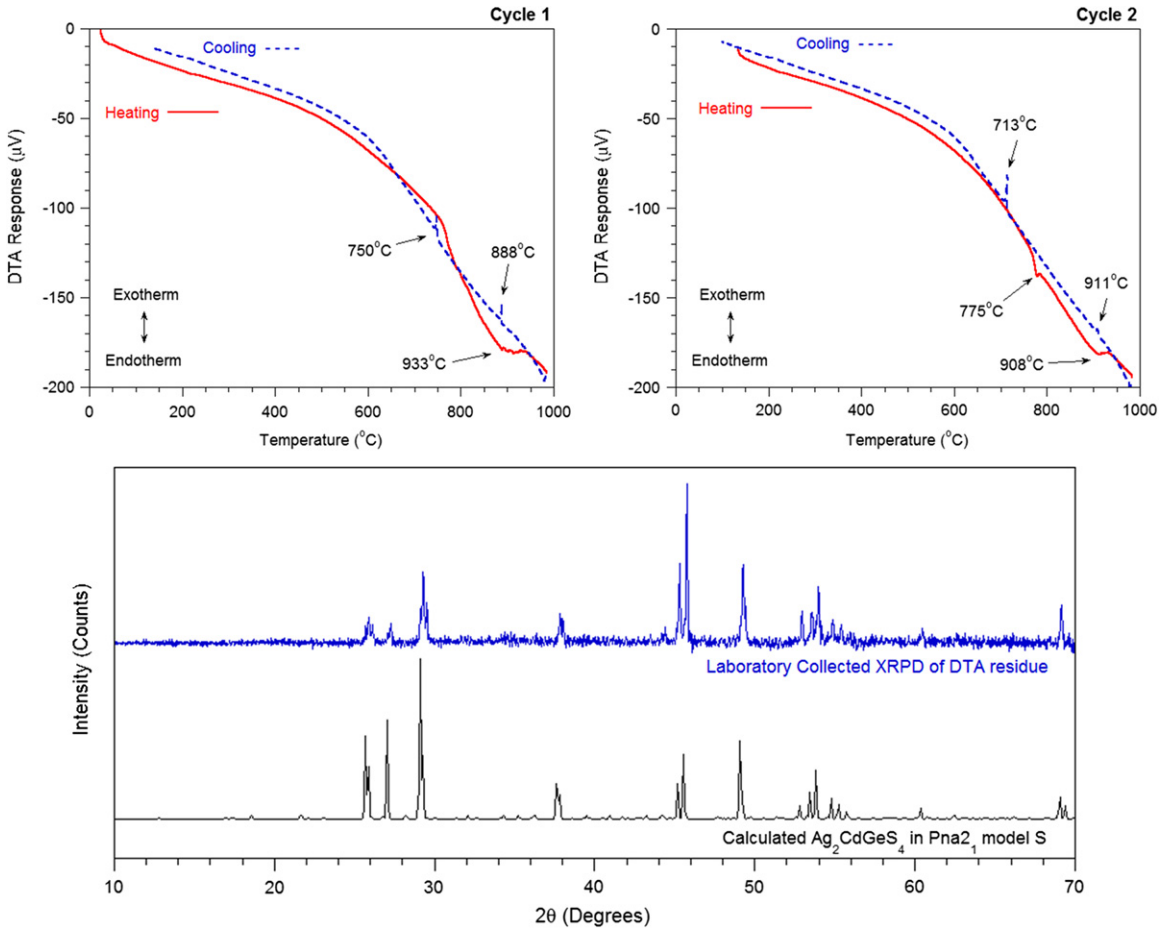

Fig. 6. Differential thermal analysis of Ag_2CdGeS_4 with heating cycles displayed with a solid line and cooling cycles with a dashed line (top). The observed X-ray powder diffraction pattern of the residue is compared to the calculated pattern for Ag_2CdGeS_4 in *Pna*2_1 (model S) (bottom).

3.5. *Optical diffuse reflectance spectroscopy*

Optical diffuse reflectance UV/vis/NIR spectroscopy was performed for Ag_2CdGeS_4 in order to estimate the band gap. The resulting spectrum shows an estimated band gap of 2.32 eV, in agreement with the orange color observed for these crystals, Fig. 7. The presence of only one clean absorption edge supports the X-ray powder diffraction analysis indicating that the sample is nearly phase pure.

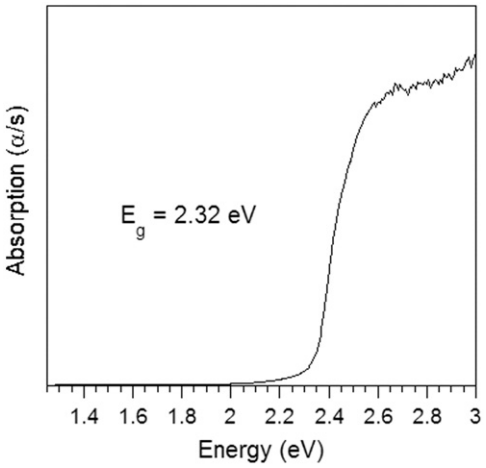

Fig. 7. Optical diffuse reflectance UV/vis/NIR spectrum converted to absorption for Ag_2CdGeS_4.

4. Conclusions [58,59]

Single crystals of the diamond-like compound Ag_2CdGeS_4 have been prepared and the structure solved and refined in the space group $Pna2_1$, although two other space groups have been previously proposed for this material. The structure determination of Ag_2CdGeS_4 was challenging due to Ag^{1+} and Cd^{2+} being isoelectronic; however careful analysis of high-quality single crystal and high-resolution synchrotron X-ray powder diffraction data provided significant clues leading to the elucidation of the most probable structure. Model S is clearly favored by the single crystal X-ray diffraction data; however model P makes chemical sense and cannot be distinguished by X-ray powder diffraction data. In fact the structure solution from synchrotron X-ray powder diffraction is a valid structure and would have been acceptable if a single crystal model had not been determined. Additionally, the possible presence of multiple polymorphs is suggested by thermal analysis. A partially disordered model was discarded due to the violation of Pauling's second and fifth rules and the observation of normal bonding distances in this material. While this compound could be a candidate for neutron diffraction studies, the synthesis is challenging, neither a single crystal of appropriate dimensions or a large enough quantity of powder has been successfully prepared, and cadmium is not a neutron-friendly element. Future studies will be aimed at preparing the material in pure form, so that it may be further studied (e.g. anomalous dispersion) without the pain-staking, added step of hand-picking the crystals.

Supporting information

Further details of the crystal structure investigation may be obtained from Fachinformationszentrum Karlsruhe, 76344 Eggenstein-Leopoldshafen, Germany (fax: (+49)7247 808 666; Email: crysdata@fiz-karlsruhe.de, http://www.fiz-karlsruhe.de/request_for_deposited_data.html. CSD number 423404).

Acknowledgments

Funding for this research was supplied by the National Science Foundation (NSF) CAREER Award Grant no. DMR-0645304. Instrumentation was purchased through NSF grants, DUE-0511444 for the X-ray powder diffractometer and MRI-CHE-0923183 for the SEM. We gratefully acknowledge Dr. Kristin L. Bunker, Mr. James Marquis and RJ Lee Group, Inc. Monroeville, PA for training and use of the digital microscope system. Use of the Advanced Photon Source at Argonne National Laboratory was supported by the U.S. Department of Energy, Office of Science, Office of Basic Energy Sciences, under Contract no. DE-AC02-06CH11357. The authors would also like to thank Dr. Brian H. Toby and Dr. Matthew Suchomel from Argonne National Laboratory for the assistance at the APS. We also thank Dr. Jim Kaduk of Polycrystallography Inc. and Dr. Cora Lind from the University of Toledo for insight into the Rietveld refinement.

References

[1] E. Parthé, Crystal Chemistry of Tetrahedral Structures, Gordon and Breach Science Publishers, New York, NY, 1964.
[2] N.A. Goryunova, in: J.C. Anderson (Ed.), The Chemistry of Diamond-like Semiconductors, The M.I.T. Press, Cambridge, 1965. chs. 1–3.
[3] J.W. Lekse, B.M. Leverett, C.H. Lake, J.A. Aitken, J. Solid State Chem. 181 (2008) 3217–3222.
[4] S. Levcenco, D. Dumcenco, Y.S. Huang, E. Arushanov, V. Tezlevan, J. Alloys Compd. 509 (2011) 7105–7108.
[5] K.A. Rosmus, J.A. Aitken, Acta Cryst. E67 (2011) i28.
[6] Q. Guo, G.M. Ford, W.C. Yang, B.C. Walker, E.A. Stach, H.W. Hillhouse, R. Agrawal, J. Am. Chem. Soc. 132 (2010) 17384–17386.
[7] G.M. Ford, Q. Guo, R. Agrawal, H.W. Hillhouse, Chem. Mater. 23 (2011) 2626–2629.
[8] S. Nakamura, T. Maeda, T. Wada, Jpn. J. Appl. Phys. 50 (2011) 05FF01.
[9] C. Rincón, M. Quintero, E. Moreno, C. Power, E. Quintero, J.A. Henao, M.A. Macías, G.E. Delgado, R. Tovar, M. Morocoima, Solid State Commun. 151 (2011) 947–951.
[10] J.W. Lekse, M.A. Moreau, K.L. McNerny, J. Yeon, P.S. Halasyamani, J.A. Aitken, Inorg. Chem. 48 (2009) 7516–7518.
[11] Y. Li, W. Fan, H. Sun, X. Cheng, P. Li, X. Zhao, J. Phys. Condens. Matter. 23 (2011) 225401.
[12] M.L. Liu, I.W. Chen, F.Q. Huang, L.D. Chen, Adv. Mater. 21 (2009) 3808–3812.
[13] X.I. Shi, F.Q. Huang, M.L. Liu, L.D. Chen, Appl. Phys. Lett. 94 (2009) 122103.
[14] F.P. Bundy, J.S. Kasper, J. Chem. Phys. 46 (1967) 3437–3446.
[15] L. Pauling, J. Am. Chem. Soc. 51 (1929) 1010–1026.
[16] J.L. Shay, J.H. Wernick, Ternary Chalcopyrite Semiconductors: Growth, Electronic Properties, and Applications, Pergamon Press, Elmsford, NY, 1975.
[17] E. Parthé, Intermetallic Compounds: Vol 1, Principles, John Wiley and Sons, New York, NY, 1994.
[18] G.H. McCabe, T. Fries, M.T. Liu, Y. Shapira, L.R. Ram-Mohan, R. Kershaw, A. Wold, C. Fau, M. Averous, E.J. McNiff, Phys. Rev. B 56 (1997) 6673–6680.
[19] H. Honig, H. Shen, G. Yao, K. Doverspike, R. Kershaw, K. Dwight, A. Wold, Mater. Res. Bull. 32 (1998) 307–312.
[20] A.B. Ellis, M.J. Geselbracht, B.L. Johnson, G.C. Lisensky, W.R. Robinson, Teaching General Chemistry: A Materials Science Companion, American Chemical Society, Washington, DC, 1993.
[21] G.C. Catella, D. Burlage, MRS Bull. 23 (1998) 28–36.
[22] S.J. Pearton, C.R. Abernathy, D.P. Norton, A.F. Hebard, Y.D. Park, L.A. Boatner, J.D. Budai, Mater. Sci Eng. R (2003) 137–168.
[23] M.C. Ohmer, R. Pandey, MRS Bull. 23 (1998) 16–20.
[24] A. Goetzberger, C. Hebling, H. Schock, Mater. Sci. Eng. 40 (2003) 1–46.
[25] S.A. Chambers, Y.K. Yoo, MRS Bull. 28 (2003) 706–707.
[26] C. Sevik, T. Çağin, Phys. Rev. B 82 (2010) 045202.
[27] E. Parthé, K. Yvon, R.H. Deitch, Acta Cryst. B25 (1969) 1164–1174.
[28] O.V. Parasyuk, L.V. Piskach, Polish J. Chem. 72 (1998) 966–968.
[29] O.V. Parasyuk, I.D. Olekseyuk, L.V. Piskach, S.V. Volkov, V.I. Pekhnyo, J. Alloys Compd. 399 (2005) 173–177.
[30] O.V. Parasyuk, L.V. Piskach, I.D. Olekseyuk, V.I. Pekhnyo, J. Alloys Compd. 397 (2005) 95–98.
[31] W. Schäfer, R. Nitsche, Mater. Res. Bull. 9 (1974) 645–654.
[32] S. Chen, A. Walsh, Y. Luo, J.H. Yang, X.G. Gong, S.H. Wei, Phys. Rev. B 82 (2010) 195203.
[33] G. Eulenberger, Monatsh. Chem. 108 (1977) 901–913.
[34] Bruker, SMART and SAINT, Bruker AXS Inc., Madison, Wisconsin, USA, 1998.
[35] G.M. Sheldrick, SADABS, University of Göttingen, Germany, 2002.
[36] Bruker, SHELXTL-PC, Release 6.14, Bruker AXS Inc., Madison, Wisconsin, USA, 2007.
[37] A. Altomare, M. Camalli, C. Cuocci, C. Giacovazzo, A. Moliterni, R. Rizzi, J. Appl. Cryst. 42 (2009) 1197–1202.
[38] A.C. Larson, R.B. Von Dreele, Los Alamos National Laboratory Report LAUR.
[39] B.H. Toby, J. Appl. Crystallogr. 34 (2001) 210–213.
[40] W.C. Hamilton, Acta Cryst. 18 (1965) 502–510.
[41] M.F.C. Ladd, R.A. Palmer, Structure Determination by X-ray Crystallography, 3rd ed., Plenum Press, New York, NY, 1994.
[42] J. Wang, B.H. Toby, P.L. Lee, L. Ribaud, S. Antao, C. Kurtz, M. Ramanathan, R.B. Von Dreele, M.A. Beno, Rev. Sci. Instrum. 79 (2008) 085105.

[43] P.L. Lee, D. Shu, M. Ramanathan, C. Preissner, J. Wang, M.A. Beno, R.B. Von Dreele, L. Ribaud, C. Kurtz, S.M. Antao, X. Jiao, B.H. Toby, J. Synchrotron Radiat. 15 (2008) 427–432.
[44] L.R. Dalesio, J.O. Hill, M. Kraimer, S. Lewis, D. Murray, S. Hunt, W. Watson, M. Clausen, J. Dalesio, Nucl. Instrum. Methods Phys. Res., Sect. A 352 (1994) 184–197.
[45] M. Abramowitz, I.A. Stegun (Eds.), Handbook of Mathematical Functions, Dover Publications, Dover, NY, 1965. (Ch. 22).
[46] P. Kubelka, F. Munk, Zeit. Für Tekn. Phys. 12 (1931) 593–605.
[47] A.J.C. Wilson, E. Prince (Eds.), International Tables of Crystallography: Volume C Mathematical, Physical, and Chemical Tables, second ed., Kluwer Academic Publishers, Boston, MA, 1999.
[48] N.V. Pervukhina, V.V. Atuchin, O.V. Parasyuk, Acta Cryst. E61 (2005) i91–i93.
[49] O.V. Parasyuk, S.I. Chykhrij, V.V. Bozhko, L.V. Piskach, M.S. Bogdanyuk, I.D. Olekseyuk, L.V. Bulatetska, V.I. Pekhnyo, J. Alloys Compd. 399 (2005) 32–37.
[50] O.V. Parasyuk, A.O. Fedorchuk, Yu.M. Kogut, L.V. Piskach, I.D. Olekseyuk, J. Alloys Compd. 500 (2010) 26–29.
[51] O.V. Parasyuk, Y.E. Romanyuk, I.D. Olekseyuk, J. Cryst. Growth 275 (2005) 159–162.
[52] H. Yamaguchi, K. Akatsuka, M. Setoguchi, Y. Takaki, Acta Cryst. B B35 (1979) 2680–2682.
[53] G. Delgado, A.J. Mora, C. Pineda, T. Tinoco, Mater. Res. Bull. 36 (2001) 2507–2517.
[54] J. Leal-Gonzalez, S.S. Melibary, A.J. Smith, Acta Cryst. 46 (1990) 2017–2019.
[55] G.E. Davidyuk, O.V. Parasyuk, S.A. Semenyuk, Y.E. Romanyuk, Inorg. Mater. 39 (2003) 919–923.
[56] C.A. Joubert-Bettan, R. Lachenal, E.F. Bertaut, E. Parthé, J. Solid State Chem. 1 (1969) 1–5.
[57] Th. Hahn (Ed.), International Tables for Crystallography: Volume A Space-Group Symmetry, fifth ed., Kluwer Academic Publishers, Boston, MA, 2002.
[58] G.Y. Chao, R.A. Gault, Can. Mineral. 38 (1998) 775–778.
[59] A.A. Vaipolin, Yu.V. Rud, I.V. Rozhdestvenskaya, Cryst. Res. Technol. 23 (1988) 337–341.